J Solid State Electrochem
DOI 10.1007/s10008-016-3324-2

ORIGINAL PAPER

Control of the LiFePO4 electrochemical properties using low-cost iron precursor in a melt process

M. Talebi-Esfandarani[1] · S. Rousselot[1] · M. Gauthier[1] · P. Sauriol[2] · M. Duttine[3] · A. Wattiaux[3] · Y. Liu[4] · A. X. Sun[4] · G. Liang[5] · M. Dollé[1]

Received: 23 January 2016 / Revised: 28 June 2016 / Accepted: 6 July 2016

Abstract $LiFePO_4$ was prepared from low-cost iron ore concentrate (containing 4.48 wt.% SiO_2 and MgO, CaO and Al_2O_3 below 0.5 wt.% as contaminant) using a melt synthesis. X-ray diffraction (XRD) refinement associated with Mössbauer spectroscopy and scanning electron microscopy-energy dispersive spectroscopy (SEM-EDX) analyses are used to track the location of Si in the material. It is shown that the iron content in the melt can be used as a means to control the doping rate of elements from iron ore concentrate (IOC) precursor according to the formula $(Li_{1-z}A_z)(Fe_{1-y}M_y)(P_{1-x}Si_x)O_4$. Electrochemical behavior of the material is affected by the doping of $LiFePO_4$. While capacity is decreased in doped material, the cycling stability is much improved. When dopants are out of $LiFePO_4$ structure, capacity retention dramatically drops as well as capacity due to the gravimetric impact of impurity phases. A trade-off between high capacity and best cycling performance is necessary. For instance, slight lack of iron in the melt (6 % deficiency) leads to a capacity only 2 % lower than that of pure Fe_2O_3-based material for the same stoichiometry and fairly good capacity retention.

Keywords $LiFePO_4$ · Melt synthesis · Iron ore concentrate · Compositions · Impurities

✉ M. Dollé
mickael.dolle@umontreal.ca

[1] Department of Chemistry, University of Montreal, Montreal, Quebec H3T 1J4, Canada

[2] Department of Chemical Engineering, Ecole Polytechnique de Montreal, H3C 3A7, Montreal, Quebec, Canada

[3] Institut de Chimie de la Matière Condensée de Bordeaux, CNRS-Université de Bordeaux, 33608 Pessac Cedex, France

[4] University of Western Ontario, N6A 5B8, London, Ontario, Canada

[5] Johnson Matthey Battery Materials Ltd., Candiac, Quebec J5R 6X1, Canada

Introduction

Challenges with global warming and pollution associated with depletion of fossil fuel resources are a great incentive to develop and use electric vehicles (EVs) and plug-in hybrid electric vehicles (PHEVs), working with batteries [1]. Lithium ion batteries are recognized as a proper choice because of its features such as high energy density, a long cyclic life, and stability in addition to mature technology [2]. However, it has some issue including cost and safety which are linked to the materials used inside batteries, especially for the cathode part [3–5]. Therefore, scientific groups have been trying to find new type of materials which can obtain better performance with lower cost and better safety to replace $LiCoO_2$ cathode material found in the first lithium ion batteries [6–8]. Since 1997, $LiFePO_4$ was established as a promising candidate for the next generation of cathode materials in lithium ion batteries because of its superior capacity retention, low cost, abundance in nature of its constituting elements, being environmentally friendly, excellent thermal stability, and high cyclability [9, 10]. Despite these advantages, pristine $LiFePO_4$ suffers from low electrical conductivity and poor ion diffusion which limits its usage in large devices [11, 12]. Different strategies can be employed such as the particle size reduction, carbon coating of particles and metal doping to overcome these drawbacks [13–17].

Many synthesis methods have been used for preparing $LiFePO_4$ including solid state, sol-gel, hydrothermal, co-precipitation, and microwave [18–22]. The main issue of these methods is that pure and fairly expensive precursors such as $FePO_4$ or FeC_2O_4 are required to achieve pure and high-

Published online: 14 July 2016

quality material [23, 24]. Generally speaking, low-cost $LiFePO_4$ with high quality is necessary for the next generation of lithium-ion batteries. Some recent studies focus on using Fe-P waste slag for the production of low-cost $LiFePO_4$ via several grinding and milling steps [25]. Gauthier et al. reported on the melt synthesis which is believed to be a quick and low-cost process for preparing $LiFePO_4$ material [26, 27]. Melt synthesis combines ideal-liquid phase reaction with short dwell times and fast reaction kinetics in a reducing atmosphere [27–29]. Our group recently made an effort to reduce the high manufacturing cost of $LiFePO_4$ by melt synthesis, using less pure non-expensive raw materials, namely iron ore concentrate as iron source [30]. However, iron ore concentrate contains some element impurities mainly SiO_2 (4.48 %), according to its chemical composition reported in a previous paper [30]. Results indicated that Si enables other cations to insert in the material structure according to "$Li(Fe_{1-y}M_y)(P_{1-x}Si_x)O_4$." Surprisingly, cycling performance was improved. The results are in agreement with other reports in the literature [31]. However, our previous work showed that insertion of doping elements in the olivine structure for a stoichiometric reactant mixture with iron ore concentrate as source of Fe led to a 7 % capacity decrease in comparison with $LiFePO_4$ synthesized using pure raw material [30].

The best composition was not optimized for synthesis of $LiFePO_4$ using iron ore concentrate in the previous work, and consequently, some impurities have formed such as Li_3PO_4 and $Li_4P_2O_7$ during synthesis [30]. These impurities act as inert and inactive mass, which reduce consequently the electrochemical performance of $LiFePO_4$ material [32]. This confirmed that material purification is needed to achieve the highest electrochemical performances. The material could thus benefit from a better control of the melt composition. Therefore, in this work, $LiFePO_4$ has been prepared by melt synthesis using non-expensive iron ore concentrate with various stoichiometric ratios. The effect of different melt compositions on the phase purity, morphology, and electrochemical properties of $LiFePO_4$ material are investigated. This work is part of an Automotive Partnership of Canada supported program to develop and pilot the molten-synthesis process to make high purity C-$LiFePO_4$ with excellent electrochemical properties for using as a cathode material in Li-ion batteries for EVs and PHEVs application.

Experimental

Synthesis of $LiFePO_4$

$LiFePO_4$ was synthesized by the melt process described in our previous work [30]. The chemical compositions of the iron ore precursor including its impurities were also reported with details in our previous paper [30]. Precise amount of $LiPO_3$ made from dehydration of LiH_2PO_4 (from TQC), iron ore concentrate (IOC; from Rio Tinto) and Fe^0 (Atomet 1001HP from Rio Tinto-QMP) were mixed together according to different compositions as shown in Table 1 and then placed in a graphite crucible. Using $LiPO_3$ as reference precursor, IOC and Fe^0 were added so that overall Fe stoichiometric ratios are comprised within a range 0.85 to 1.13. IOC is added based on its Fe content, whereas Fe^0 amount is used as a Fe^{3+}-reducing agent, according to $Fe_2^{3+}O_3 + Fe^0 \rightarrow 3Fe^{2+}O$. The use of $LiPO_3$ precursor allows the simultaneous addition of Li and P contents. However, for Li-rich and P-rich materials, Li_2CO_3 (from FMC Lithium Co.) and $NH_4H_2PO_4$ (from Newhonte (Wuhan) Industry & Trade Co., LTD) were used as extra Li and P sources, respectively. It is important to note that the amount of SiO_2 coming from iron ore concentrate is the same for all the $LiFePO_4$ synthesized samples. The impact of the presence of SiO_2 has already been demonstrated when using IOC or in the case of co-doping [30, 31]. In the present case, its amount was controlled in order to focus only on the variation of Fe content. Some carbon black, *ca.* 200 ± 50 mg, was used to avoid oxidation of iron during synthesis. The crucibles were heated at 1100 °C for 3 h and then quenched to room temperature under nitrogen atmosphere to obtain $LiFePO_4$ ingots. For the sake of comparison, some samples were prepared using pure Fe_2O_3 (Sigma-Aldrich) in the same compositions.

Material characterizations

For material characterization, the ingots were cut in half. One part was ground with a mortar and a pestle to obtain micrometer-sized $LiFePO_4$ powder. A part of ingots was kept as is and mounted in a conductive resin and then polished with different papers and pastes. The microstructure and elemental mapping of mounted samples was examined by a scanning electron microscope SEM-Hitachi S-4800 equipped with energy dispersive spectroscopies (EDXs). The materials end composition matched with expected composition as it was analyzed by ICP-MS. This indicates no Li evaporation occurs during synthesis in the current melt protocol. The crystal structure of the ground powders was analyzed by X-ray diffraction (XRD) using a Bruker D8 Advance X-ray diffractometer equipped with Cu Kα radiation source. XRD measurements were collected in steps of 0.02° in 2θ range of 10–80°. The unit cell parameters of the prepared powders were determined using the Le Bail method (pattern matching) with the program FullProf Suite. Mössbauer spectra were recorded in transmission geometry using a constant acceleration Halder-type spectrometer with a room temperature ^{57}Co source (Rh matrix). The velocity scale was calibrated using a pure metal iron foil. The polycrystalline absorbers containing about 10 mg/cm^2 of iron were placed into a sample holder in order

to collect ^{57}Fe Mössbauer spectra at 293 K. Refinement of the Mössbauer hyperfine parameters (δ isomer shift, Δ quadrupole splitting, ε quadrupole shift, H hyperfine field, Γ signal linewidth and relative areas) was performed using homemade programs and the WinNormos® software [33]. A continuous-flow agitator wet mill (Netszch Microcer) was used for further grinding of powders down to nanometer-size. The solvent was isopropyl alcohol (IPA) to avoid any undesired dissolution of the active material in the solvent. The slurry in the ratio 5:95 ([solid content]:[solvent] by weight) passed through the mill containing 200 mL 0.5 mm yttria-stabilized zirconia beads. Milling was carried out for 3 h. Lactose (11 % relative to the $LiFePO_4$ weight) was added to slurry during milling as a carbon source. Afterwards, the mixture was collected from the mill and the solvent allowed to evaporate on hot plate. The powder was then annealed at 700 °C for 2 h in a nitrogen atmosphere to complete the carbonization of β-lactose to achieve $LiFePO_4$/C. The specific surface area of the powders was determined by the Brunauer, Emmett, Teller (BET) method (Micromeritics Gemini 2380). Carbon content of powders was measured using a LECO C/S analyzer (LECO-SC632).

Electrochemical characterization

The electrodes for electrochemical evaluations were fabricated by combining 83 wt.% of the $LiFePO_4$/C powder, 9 wt.% of carbon black Timcal C65, and 8 wt.% of polyvinylidene difluoride (PVDF) in *N*-methyl pyrrolidone (NMP) solvent to form a slurry. The slurry was mixed for few hours to homogeneity and spread on a carbon-coated aluminum foil using the doctor blade method. After drying at 70 °C in a vacuum oven overnight, electrode disks of 2.5 ± 0.5 mg/cm^2 loading were cut and pressed. Standard coin cells (2032) were assembled in an Ar-filled glove box. A lithium foil was used as the anode and a Celgard2400 as separator. The electrolyte was 1 M $LiPF_6$ in ethylene carbonate and diethyl carbonate (1:2 volume ratio) solvents. The electrochemical performances were determined on the cells between 2.2 and 4.0 V vs. Li^+/Li at different current rates using a VMP electrochemical station (Biologic, France). All the electrochemical measurements were performed at room temperature. For each sample, three cells were assembled to insure reproducibility. Capacity variations lower than 1 mAh/g were found for every 3-cell set. For each sample, the capacity is expressed in function of the uncoated material as obtained.

Results and discussion

The XRD patterns of IOC-based materials synthesized with different compositions are presented in Fig. 1a, b. For all samples, the main diffraction peaks can be indexed by an orthorhombic olivine-type structure with the *Pnma* space group (JCPDS 40-1499) corresponding to $LiFePO_4$. In the case of melts with iron excess (i.e., 13 and 4 % excess), iron or iron phosphide inclusions were found at the bottom of the ingots as shown in Fig. 2. Moreover, traces of Fe_xP phase were identified on the side of the graphite crucibles. All iron bits were collected using magnet. Obviously for lower iron content, no Fe^0 was detected from the materials. Different types of impurity phases were detected according to the melt composition. In the case of Fe excess in the melt, Li_3PO_4 impurity phase is clearly visible. The existence of Li_3PO_4 phase can be surprising since these melts are Li and P deficient. However, the formation of Fe_xP phase remaining on the wall of the crucible and "unreacted" Fe bits can explain why Li_3PO_4 can grow in the melt. The presence of Li_3PO_4 phase is even more obvious in the case of Li excess in Fig. 1b. The phase tends to vanish when Fe concentration decreases in the melt as

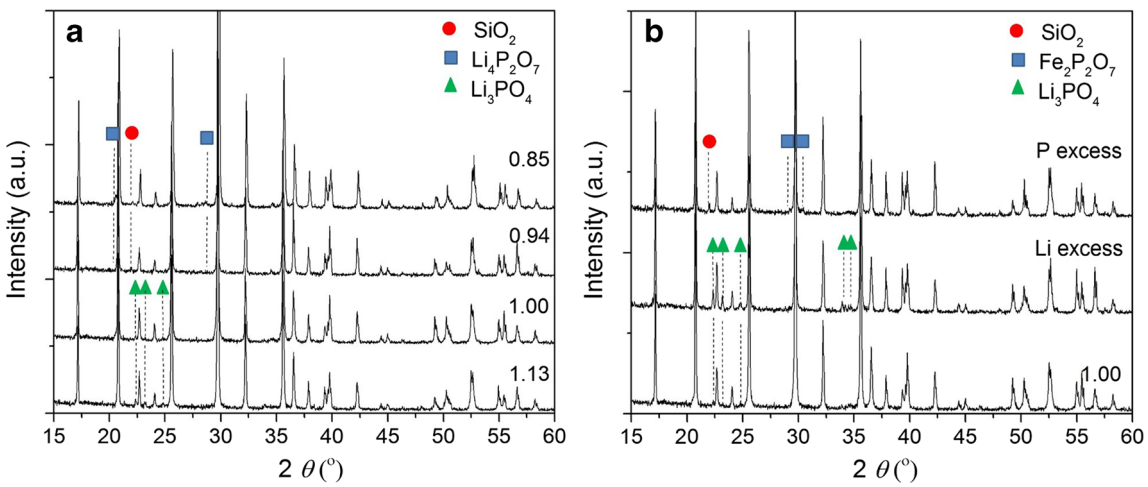

Fig. 1 **a**, **b** XRD patterns of the IOC-based materials synthesized with different compositions

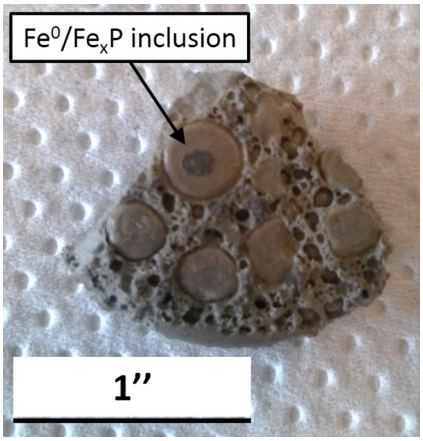

Fig. 2 Iron or iron phosphide inclusions found at the bottom of the ingots made from iron excess composition

seen from Fig. 1a. Above a stoichiometric melt, by increasing $LiPO_3$ content in the starting melt (i.e., 6 and 15 % deficiency in Fe), $Li_4P_2O_7$ impurity phase starts to grow. Li_3PO_4-$LiPO_3$ phase diagram indeed shows that $Li_4P_2O_7$ is a congruent phase of 50 % Li_3PO_4/50 % $LiPO_3$ [34]. No other impurities, related to Fe, such as Fe_xP, $Fe_2P_2O_7$, nor NASICON ($Li_3Fe_2(PO_4)_3$) phases were detected on the patterns in Fig. 1a. The use of a graphite crucible and a carbon black layer on top of the melt during synthesis generates a reducing atmosphere to prevent formation of NASICON as reported in [30]. This is further confirmed by Mössbauer measurement shown in Fig. 4 where no impurity related to Fe is detected. This is described in more detail below. However, for all the samples in Fig. 1a, the ratio between Li/P was kept 1:1; complementary information can be deduced when changing this ratio as shown in Fig. 1b. A small amount of $Fe_2P_2O_7$ is detected in a sample with a P excess (Fig. 1b). Growth of $Fe_2P_2O_7$ impurity is indeed expected in Li-deficient materials [29]. However, no $Fe_3(PO_4)_2$ phase is identified as opposed to earlier work on samples with Li-deficient samples [35]. In contrast, more Li_3PO_4 was found in samples with $Li/P > 1$.

As reported in [30], the solidified materials contain impurity elements, mainly Si, coming from the iron ore concentrate used as Fe precursor. No silica or silicate phase is seen on the patterns in the case of Fe excess samples, from 1.13 to 1.04, despite its slightly higher amount. In contrast with a decrease of Fe concentration in the melt, a slight peak at $2\theta = 22.0°$ appears as indicated in Fig. 1a. This peak is ascribed to cristobalite SiO_2 phase (JCPDS file 39-1425). The situation is clearer for samples with $Li/P < 1$ shown in Fig. 1b where SiO_2-related peak is well observed. This impurity phase was previously identified in a sample made from stoichiometric melt only after a thermal treatment up to 900 °C [30]. This suggests that the behavior of SiO_2 is linked with the melt compositions. Further understanding on the doping of $LiFePO_4$ was possible using full-pattern matching with Le Bail method to calculate the lattice parameters and cell volume. Rietveld refinement is unfortunately not a suitable method in the present study for the reasons discussed in [30]. The results of the lattice parameters and unit cells are listed in Table 1 for the different compositions using IOC or Fe_2O_3 as precursors. Figure 3 summarizes this table by plotting of the lattice volume for each sample as a function of the iron stoichiometry in the melt. For Fe_2O_3 precursor, the lattice volume is unchanged whatever the iron stoichiometry in the studied range at 291.25 ± 0.01 Å^3. In contrast, the cell volume is highly dependent on the melt composition for IOC case. The cell volume is first stable at the same value as the lattice of Fe_2O_3-based samples up to 0.94-IOC composition. When IOC stoichiometry in the melt increases further, this value rises up to 291.94(3) Å^3 for the 1.13-IOC sample. Such lattice volume increase can be explained by two main hypotheses.

Table 1 Unit cell of samples from Whole Pattern Matching

Series	Sample	[Li]	[Fe]	[P]	*a* (Å)	*b* (Å)	*c* (Å)	Volume (Å^3)
IOC	1.13-IOC	1	1.13	1	10.3429 (7)	6.0101 (4)	4.6965 (3)	291.94 (3)
	1.04-IOC	1	1.04	1	10.3399 (4)	6.0102 (3)	4.6946 (2)	291.75 (2)
	1.00-IOC	1	1.00	1	10.3340 (4)	6.0076 (2)	4.6935 (2)	291.39 (2)
	0.94-IOC	1	0.94	1	10.3334 (4)	6.0064 (3)	4.6932 (2)	291.29 (2)
	0.89-IOC	1	0.89	1	10.3331 (5)	6.0078 (3)	4.6917 (3)	291.26 (3)
	0.85-IOC	1	0.85	1	10.3325 (4)	6.0076 (2)	4.6922 (2)	291.26 (2)
	Li excess	1.07	1.00	1	10.3343 (4)	6.0080 (2)	4.6929 (2)	291.38 (2)
	P excess	1	1.00	1.07	10.3344 (5)	6.0072 (3)	4.6938 (2)	291.40 (2)
Fe_2O_3	1.04-Fe_2O_3	1	1.04	1	10.3333 (3)	6.0071 (1)	4.6919 (1)	291.24 (1)
	1.00-Fe_2O_3	1	1.00	1	10.3334 (4)	6.0072 (2)	4.6921 (2)	291.26 (2)
	0.94-Fe_2O_3	1	0.94	1	10.3331 (4)	6.0072 (2)	4.6921 (2)	291.25 (2)

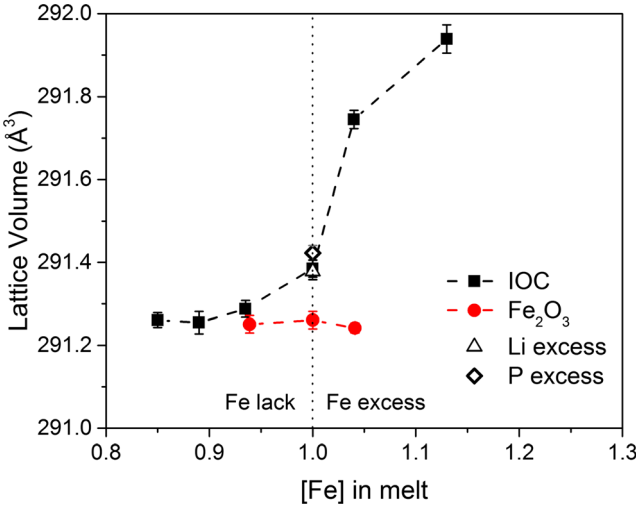

Fig. 3 Plot of the lattice volume for each sample series as a function of the iron stoichiometry in the melt

On one hand, lattice increase was shown to be possibly related to disordering in the $LiFePO_4$ structure [35, 36], which can be described as $M_1M_2PO_4$ with Li ions (on the M_1 site) and Fe ions (on the M_2 site). Excessive iron in hydrothermally synthesized materials partially occupies M_1 sites while M_2 site remains fully occupied by Fe, causing the $LiFePO_4$ lattice parameters to increase. Sub-stoichiometric samples showing anti-site mixing of Li^+ and Fe^{2+} can also lead to a noticeable increase of unit cell volume starting from 6 % M_1 vacancies and 3 % Fe on M_1 site [35]. In order to identify Fe position, Mössbauer measurements were undertaken on samples with either iron excess or iron deficiency made from IOC precursor

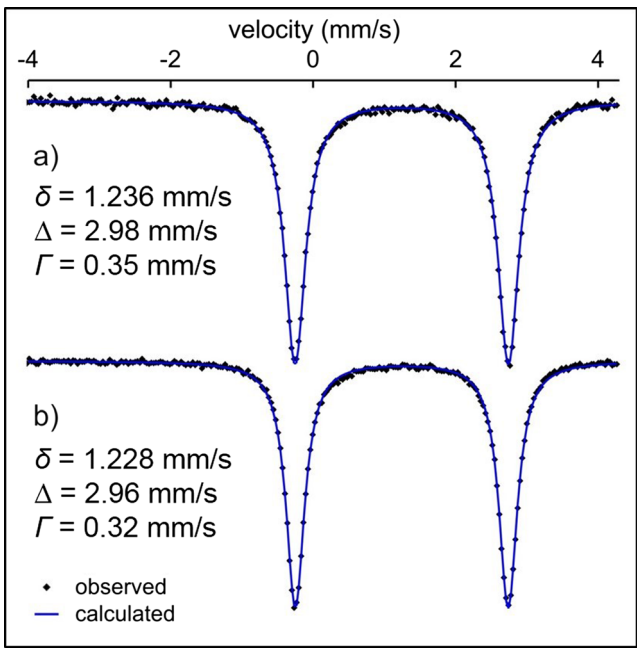

Fig. 4 Mössbauer spectra of samples with **a** iron excess IOC-1.04, **b** iron deficiency IOC-0.94 made from IOC precursor

as shown in Fig. 4. In every case, the spectra present only one symmetric Fe component with the very same isomer shift δ of 1.23 mm/s and quadrupole splitting Δ of 2.97 mm/s. This component can be ascribed to Fe^{2+} in octahedral environment in $LiFePO_4$ [10, 36–38]. These observations exclude the presence of Fe^{2+} in M_1 site or Fe^{3+} in M_1 and M_2 sites as reported elsewhere in the case of $LiFePO_4$ prepared using different synthesis methods [10, 36–38]. This means that no anti-site mixing is found in all of the present samples. It has to be noted though that the full width at half maximum, Γ, is rather high compared to what is observed in solid-state synthesized samples but is comparable to values found for hydrothermal materials [39, 40]. This may be related at some extent to disordering or the presence of structural defects around the Fe site in the LFP structure on the samples [40]. While solid-state materials in [40] were synthesized above 575 °C, hydrothermal materials in [39] were prepared at low temperature (170 °C). In the present case, the molten baths are quenched from 1100 °C to room temperature. It is estimated the material is cooled in less than 30–60 min. Fast solidification is likely to induce structural defects in the material, i.e. large distribution of Fe site. In addition, Γ is higher in the case of IOC-1.04 (0.35 mm/s) compared to IOC-0.94 (0.32 mm/s) reflecting an even more disordered structure in IOC-1.04.

On the other hand, doping of $LiFePO_4$ can result in lattice volume change [41]. In a previous study focusing on stoichiometric melts, it was reported that impurity elements from the starting Fe precursor were included as multi-substituting in the $LiFePO_4$ final structure leading to cell volume expansion [30]. Based on the XRD results and lattice parameter calculation, excess of Fe in the melt implies that Si is included in the $LiFePO_4$ structure, inducing bigger lattice parameters. In contrast, Si does not insert in the $LiFePO_4$ structure when Fe is deficient; consequently, lattice parameters are smaller and SiO_2 is detected in the XRD patterns.

SEM pictures and corresponding Si element EDX mapping were taken for different melt compositions to confirm this hypothesis as shown in Fig. 5. The presence of a matrix phase, identified as $LiFePO_4$ phase, and secondary phases in dark gray color for all samples is observed on SEM images. The proportion of secondary phases is higher for samples with lack of iron, 0.94-IOC, and 0.89-IOC. These secondary phases are P-rich and O-rich indicating the presence of $Li_4P_2O_7$ and Li_3PO_4 in agreement with XRD results. EDX mapping of Si elements on the same area shows much discrepancy according to the melt composition. For 1.00-IOC, Si is distributed homogeneously all over the sample, i.e. in $LiFePO_4$ phase and secondary phases. In a stoichiometric melt, only part of Si is included as Si^{4+} dopant in the $LiFePO_4$ structure after synthesis. The other part is under oxide form SiO_2 in amorphous state in the material as obtained and crystallized with annealing [30]. Nevertheless, in the case of 0.94-IOC and 0.89-IOC, Si tends to be concentrated in secondary phases as attested by

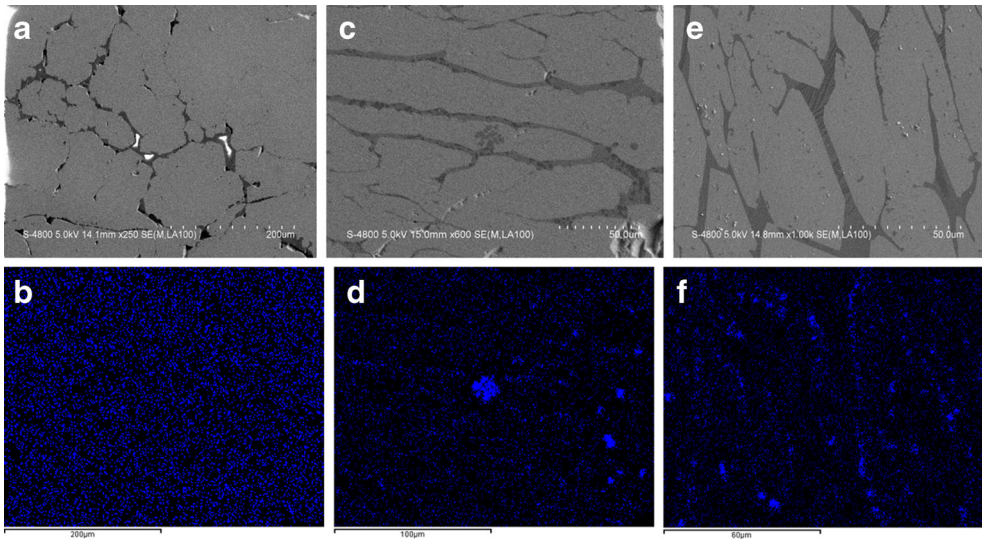

Fig. 5 SEM pictures and corresponding Si element EDX mapping for **a** and **b** IOC-1.00 , **c** and **d** IOC-0.94 and **e** and **f** IOC-0.89

the intense spots and lines in Fig. 5d, f. SEM-EDX results are in complete agreement with XRD analyses and confirm the insertion of Si^{4+} in the $LiFePO_4$ structure when Fe is in excess in the melt. SiO_2 is observed only in Fe-deficient samples; for these samples, the cell volume is the same as the one of Fe_2O_3 samples. In other words, Si ions do not insert in the $LiFePO_4$ structure in these materials. With increase of Fe in the melt, SiO_2 phase vanishes from the pattern as Si^{4+} (and other impurity element) insert in $LiFePO_4$, inducing the volume of the unit cell to increase. It is believed that Si^{4+} is located in P^{5+} site in the case of multi-doping or co-doping according to this composition $Li(Fe_{1-y}M_y)(P_{1-x}Si_x)O_4$ [30, 31]. This tends to be in agreement with the higher disordering surrounding Fe site found by Mössbauer in Fe-rich composition. P-excess and Li-excess samples support this assumption as well. SiO_2 is indeed observed on its pattern indicating that [P] increase in the melt tends to impede Si^{4+} from inserting in the olivine structure. In contrast, an increase of Li concentration does not favor the growth of SiO_2 meaning that Si^{4+} is not located in Li^+ site. For this latter sample, the extra Li does not even insert in olivine phase as the lattice volume remains constant and only results in growth of extra Li_3PO_4 impurity. The presence of Si^{4+} is "crucial" for doping as it allows balancing the electronic charge induced by other impurity elements in the olivine structure. However, a more complex composition such as $(Li_{1-z}A_z)(Fe_{1-y}M_y)(P_{1-x}Si_x)O_4$ cannot be excluded with A and M being cations present in the IOC precursor.

It has to be noted also that 4-point probe conductivity measurement was attempted on thin slice using gold blocking electrodes to evidence any improvement of the electronic conductivity with or without Si^{4+} and other cation insertions in $LiFePO_4$ structure. However, the conductivity of the samples was too low to be measured with the equipment resolution (*ca.* 10^{-8} S/cm). This indicates that if any improvement is expected due to Si^{4+} and other cation insertions in the structure, the improvement is very limited and may not induce increase of power performance.

Powders from ingots were wet-milled and further pyrolyzed for electrochemical characterization. The specific surface area of $LiFePO_4$/C samples is in the range from 20 to 45 m^2/g. The amount of carbon source, measured with carbon analyzer, is found to be 3.3 ± 0.2 % in all final materials. The galvanostatic curves at C/10 of selected samples, i.e. reference samples made from Fe_2O_3 and IOC-based samples 1.13-IOC with $Li(Fe_{1-y}M_y)(P_{1-x}Si_x)O_4$ expected composition and 0.94-IOC where doping elements are out of olivine structure, are plotted in Fig. 6. In all cases, the curves only present the flat plateau profile centered at 3.45 V vs. Li^+/Li characteristic of the two-phase redox reaction of $LiFePO_4$ and $FePO_4$. The same polarization is found at *ca.* 55 mV indicating that all

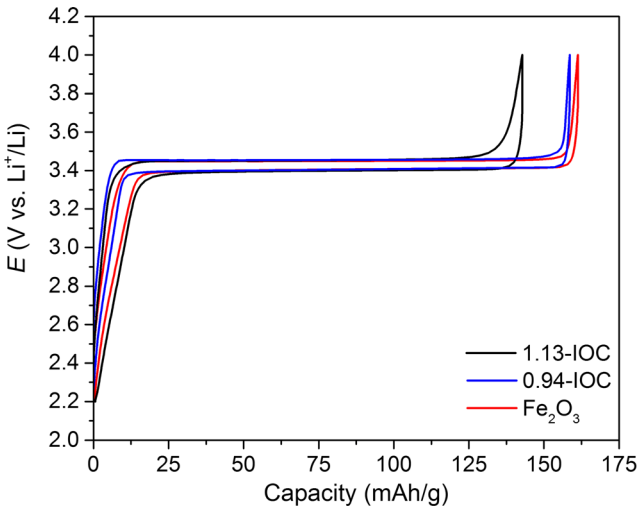

Fig. 6 The galvanostatic curves at C/10 of selected samples

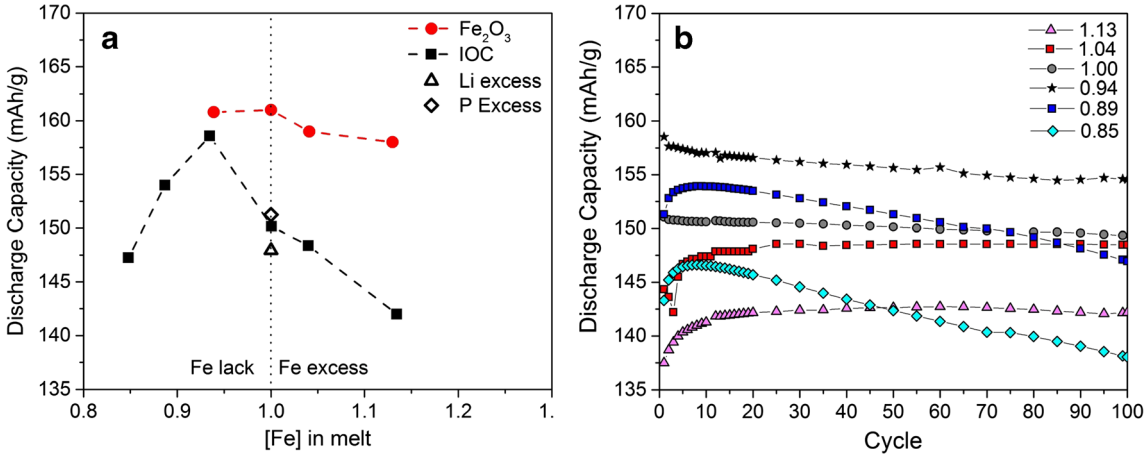

Fig. 7 **a** Maximum discharge capacity as a function of [Fe] in the melt. **b** Cycle life on 100 cycles of the samples with different melt compositions

materials are sufficiently well carbon coated for this cycling rate. The end of charge in the case of Fe_2O_3 and 0.94-IOC presents a sharp increase to the cutoff potential whereas 1.13-IOC, however, displays more kneeling. In contrast, such discrepancy is not seen for the end of discharge side. The reason for such behavior is not clear. This could be related to the nano-sized character of the material [42]. Nevertheless, with use of the same synthesis protocol and further confirmation by BET measurement, particle size difference is not expected among the samples. This might rather be linked to the presence of doping elements in the LFP structure. This question will be cleared out in an upcoming paper.

The maximum discharge capacity varies as a function of [Fe] in the melt between these last samples as it is detailed in Fig. 7a for the whole IOC and Fe_2O_3 series. The figure clearly shows that the maximum discharge capacity strongly depends on the iron stoichiometry in the melt for IOC series. Sample 1.13-IOC shows the lowest discharge capacity of 142 mAh/g. With increasing $LiPO_3$ content, the discharge capacity improved up to a maximum of 158.5 mAh/g for 0.94-IOC sample. However, further increase in $LiPO_3$ caused a quick capacity loss for samples 0.89-IOC and 0.85-IOC. Surprisingly with IOC, as opposed to the Fe_2O_3 samples, the best capacity is not found for a stoichiometric melt but for one with a slight Fe deficiency. For comparison, the discharge capacity of samples prepared with pure Fe_2O_3 is also shown in Fig. 7a. The capacity is minimally affected by the [Fe] variation in the melt in the studied range as it varies from 158 to 161 mAh/g. For both series, the samples synthesized at 0.94 exhibit discharge capacities only 2 % apart (161 and 158.5 mAh/g). This 2 % difference corresponds to the expected impurity contribution of 1.9 wt.% in 0.94-IOC sample in comparison to 0.94-Fe_2O_3. This suggests that the impurity oxides for this composition do not contribute to capacity loss more than their gravimetric impact. On both sides of this particular composition, the discharge capacity decreases. When Fe is lacking in the samples, the presence of SiO_2 is detrimental to the material electrochemical activities as explained in detail below. In the case of samples with Fe excess, impurity cations in IOC could partially substitute Li (which is missing in the melt) in M_1 site and either block Li diffusion channels or decrease the number of Li atoms available. For both assumptions, the electrochemical capacity is affected. Olivine phase in samples with $Li/P > 1$ is similar to stoichiometric composition one; however, the capacity is reduced due to an increase of the Li_3PO_4 impurity phase. In contrast, samples with $Li/P < 1$, even though Si^{4+} is essentially expelled from the olivine phase, the capacity does not significantly increase compared to the stoichiometric case. This could imply that despite Si atoms are essentially out of the $LiFePO_4$ structure, some Li diffusion channels could be blocked by larger cations in M_1 site. The electrochemical capacities of the materials are in agreement with the XRD conclusions and provide complementary information for determining the composition of olivine phase when using IOC precursor.

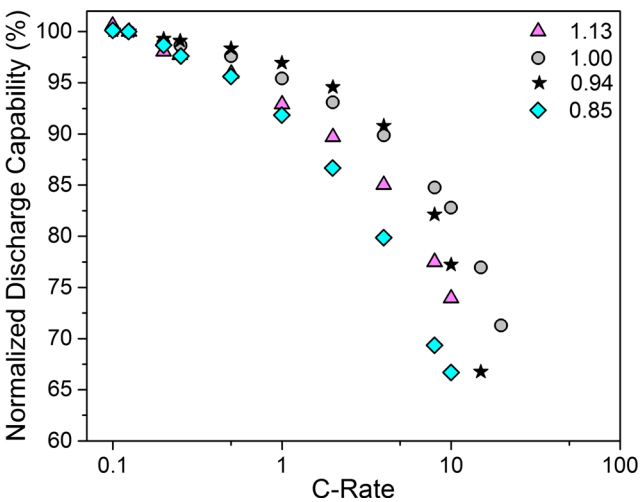

Fig. 8 Normalized discharge capability for extreme and significant samples

Figure 7b shows the cycle life on 100 cycles of the samples with different melt compositions. Coulombic efficiency for all samples in the presence of excess iron is higher than 99.5 %. Most of the samples present several activation cycles before reaching the maximum capacity. For Fe concentration in the melt above stoichiometric ratio, i.e., samples identified as "doped" $LiFePO_4$, after reaching highest capacity, no significant fade is observed. It has been measured that a capacity retention is higher than 99.6 % on 50 cycles after maximum capacity. However, with a decrease of Fe content in the melt, capacity fading is more marked. This is particularly obvious for sample 0.85-IOC. In that case, capacity retention dramatically drops close to 90 %. The improved cycle life of doped samples is in agreement with results from Nishijima et al. [31]. It is indeed reported that co-substitution of Si^{4+} for P^{5+} and Zr^{4+} for Fe^{2+} in $LiFePO_4$ structure increases the cyclability of $LiFePO_4$ powder due to reduced volume change upon delithiation/lithiation process. The present material composition $(Li_{1-z}A_z)(Fe_{1-y}M_y)(P_{1-x}Si_x)O_4$ seems to go in the same direction than the one reported by Nishijima et al. Analysis of the XRD pattern of a delithiated sample (not shown) did not evidence significant reduced volume change for doped samples. Nevertheless, considering the low content of dopant, relatively slight reduction of volume change is expected. Investigations are currently under process in order to determine more precisely the doped material composition when using IOC. Undoped samples (lack of Fe), on the other hand, contain $Li_4P_2O_7$ and SiO_2 phases. $Li_4P_2O_7$ impurity is not expected to be harmful for $LiFePO_4$ electrochemical characteristics besides its gravimetric impact on specific capacity. In contrast, SiO_2 is known to be possibly detrimental to lithium battery cycle life as it may react with $LiPF_6$ salt from electrolyte and the possible formation of HF [43]. These reasons could partly explain the poorer cycle life observed for undoped samples in the present study. However, the capacity retention of Li-excess (doped without SiO_2 phase) sample is rather low at only 94.5 % whereas the one of P-excess ("undoped" with presence of SiO_2 phase) sample is the same as for the stoichiometric sample. It is not clear at present why the capacity retention of the samples with Li excess and P excess is behaving this way; the opposite trend was expected.

Power performance was measured for the different IOC samples. Figure 8 shows the normalized discharge capability for extreme and significant samples, namely 1.13-IOC, 1.00-IOC, 0.94-IOC, and 0.85-IOC. Due to differences in capacity retention according to material composition, the capacity at 0.1C, obtained after measurement of the capacities at higher currents, is used as reference. The capacities were normalized as a mean to compare capacities from samples with different maximum specific capacities. Two sets of values appear. Samples 1.00-IOC and 0.94-IOC present the best power performance close to that of materials made from pure precursors [30]. In contrast, samples 1.13-IOC (doped) and 0.85-IOC (undoped) have somewhat lower power performance. The loss is already appearing at relatively low C-rates, *ca.* C/4. The decrease is then obviously getting more marked with increase of the C-rate up to 10C. The effect of "doping" vs. "non-doping" on the power performance is not clear then. Olivine lattice expansion observed in doped materials could lead to larger lithium diffusion channels. This could promote discharge ability at higher currents [20]. Particle size variations can also affect the power performance of the materials as increased power is found for smaller particles [20]. However, no such effect is visible when comparing doped to undoped samples with close particle size and carbon content. Instead, the power performance is slightly decreased in samples with extreme melt compositions, i.e., with more impurities, Li_3PO_4, or $Li_4P_2O_7$. Although coating of disordered Li_3PO_4 and/or $Li_4P_2O_7$ around LFP particles is recognized for possibly increasing lithium diffusion [44, 45], in the present case, such impurities appear as crystalline secondary phases and may act differently.

Conclusions

$LiFePO_4$ cathode material was synthesized using melt process with low-cost iron ore concentrate (IOC) as iron source and with variation of the Fe content in the melt. The low-cost IOC containing SiO_2 as major impurity, up to 4.48 wt.% and other oxides such as MgO and CaO below 0.5 wt.%, was used to reduce significantly the raw material cost and further compared to materials made from pure Fe_2O_3. According to refinement of XRD patterns and on the basis of Mössbauer spectroscopy results and SEM-EDX characterization, it appeared that impurity cations from IOC can insert in the LiFePO4 structure when the melt is Fe-rich according to the formula $(Li_{1-z}A_z)(Fe_{1-y}M_y)(P_{1-x}Si_x)O_4$. Control of the Fe content in the melt though allows $LiFePO_4$ structure purification. The electrochemical properties of the materials are strongly related to the insertion of dopants in $LiFePO_4$ phase. If the insertion of dopants does not significantly affect the electronic conductivity of the samples nor their power performance, material capacity and cycle life strongly depend on the doping of $LiFePO_4$ structure. Capacity retention is then best when material is doped whereas capacity is maximum with slight iron deficiency. In the particular case of 0.94-IOC, the capacity is only 2 % lower than that of the corresponding sample made from pure Fe_2O_3 precursor. This study shows that with proper control of the melt composition using low-cost IOC precursor, resulting $LiFePO_4$ phase can be purified and it is possible to achieve electrochemical performance approaching that of pure $LiFePO_4$ made from an expensive Fe_2O_3 precursor.

Acknowledgments The authors would like to thank NSERC and CFI, through the Automotive Partnership Canada program, and Johnson-Matthey Inc. for their financial support.

References

1. Arico AS, Bruce P, Scrosati B, Tarascon J-M, Van Schalkwijk W (2005) Nanostructured materials for advanced energy conversion and storage devices. Nat Mater 4(5):366–377
2. Tarascon JM, Armand M (2001) Issues and challenges facing rechargeable lithium batteries. Nature 414(6861):359–367
3. Li J, Daniel C, Wood D (2011) Materials processing for lithium-ion batteries. J Power Sources 196(5):2452–2460
4. Etacheri V, Marom R, Elazari R, Salitra G, Aurbach D (2011) Challenges in the development of advanced Li-ion batteries: a review. Energy Environ Sci 4(9):3243–3262
5. Goodenough JB, Kim Y (2011) Challenges for rechargeable batteries. J Power Sources 196(16):6688–6694
6. Mizushima K, Jones PC, Wiseman PJ, Goodenough JB (1980) LixCoO2 (0<x<-1): a new cathode material for batteries of high energy density. Mater Res Bull 15(6):783–789
7. Ellis BL, Lee KT, Nazar LF (2010) Positive electrode materials for Li-ion and Li-batteries. Chem Mater 22(3):691–714
8. Song H-K, Lee KT, Kim MG, Nazar LF, Cho J (2010) Recent progress in nanostructured cathode materials for lithium secondary batteries. Adv Funct Mater 20(22):3818–3834
9. Padhi AK, Nanjundaswamy KS, Goodenough JB (1997) Phospho-olivines as positive-electrode materials for rechargeable lithium batteries. J Electrochem Soc 144(4):1188–1194
10. Yamada A, Chung SC, Hinokuma K (2001) Optimized LiFePO4 for lithium battery cathodes. J Electrochem Soc 148(3):A224–A229
11. Huang H, Yin S-C, Nazar LF (2001) Approaching theoretical capacity of LiFePO4 at room temperature at high rates. Electrochem Solid State 4(10):A170–A172
12. Ravet N, Chouinard Y, Magnan JF, Besner S, Gauthier M, Armand M (2001) Electroactivity of natural and synthetic triphylite. J Power Sources 97–98(0):503–507
13. Armand, M, Gauhtier, M, Magnan, JF, and Ravet, N 2002 Method for synthesis of carbon-coated redox materials with controlled size. WO 02/27823 A1
14. Talebi-Esfandarani M, Savadogo O (2014) Enhancement of electrochemical properties of platinum doped LiFePO4/C cathode material synthesized using hydrothermal method. Solid State Ionics 261(0):81–86
15. Doeff MM, Hu Y, Mclarnon F, Kostecki R (2003) Effect of surface carbon structure on the electrochemical performance of LiFePO4. Electrochem Solid State 6(10):A207–A209
16. Doeff MM, Wilcox JD, Kostecki R, Lau G (2006) Optimization of carbon coatings on LiFePO4. J Power Sources 163(1):180–184
17. Omenya F, Chernova NA, Zhang R, Fang J, Huang Y, Cohen F, Dobrzynski N, Senanayake S, Xu W, Whittingham MS (2012) Why substitution enhances the reactivity of LiFePO4. Chem Mater 25(1):85–89
18. Talebi-Esfandarani M, Savadogo O (2014) Synthesis and characterization of Pt-doped LiFePO4/C composites using the sol–gel method as the cathode material in lithium-ion batteries. J Appl Electrochem 44(5):555–562
19. Chen J, Bai J, Chen H, Graetz J (2011) In situ hydrothermal synthesis of LiFePO4 studied by synchrotron X-ray diffraction. J Phys Chem Lett 2(15):1874–1878
20. Zhang W-J (2010) Comparison of the rate capacities of LiFePO4 cathode materials. J Electrochem Soc 157(10):A1040–A1046
21. Omenya F, Chernova NA, Wang Q, Zhang R, Whittingham MS (2013) The structural and electrochemical impact of Li and Fe site substitution in LiFePO4. Chem Mater 25(13):2691–2699
22. Talebi-Esfandarani M, Savadogo O (2014) Effects of palladium doping on the structure and electrochemical properties of LiFePO4/C prepared using the sol-gel method. J New Mater Electrochem Syst 17(2):91–97
23. Herle PS, Ellis B, Coombs N, Nazar LF (2004) Nano-network electronic conduction in iron and nickel olivine phosphates. Nat Mater 3(3):147–152
24. Ojczyk W, Marzec J, Świerczek K, Zając W, Molenda M, Dziembaj R, Molenda J (2007) Studies of selected synthesis procedures of the conducting LiFePO4-based composite cathode materials for Li-ion batteries. J Power Sources 173(2):700–706
25. Kang H, Wang G, Guo H, Chen M, Luo C, Yan K (2012) Facile synthesis and electrochemical performance of LiFePO4/C composites using Fe–P waste slag. Ind Eng Chem Res 51(23):7923–7931
26. Gauthier L, Gauthier M, Lavoie D, Michot C, Ravet N (2003) Process for preparing electroactive insertion compounds and electrode materials obtained therefrom in US Patent 7,534,408 B2
27. Gauthier M, Michot C, Ravet N, Duchesneau M, Dufour J, Liang G, Wontcheu J, Gauthier L, Macneil DD (2010) Melt casting LiFePO4: I. Synthesis and characterization. J Electrochem Soc 157(4):A453–A462
28. Macneil DD, Devigne L, Michot C, Rodrigues I, Liang G, Gauthier M (2010) Melt casting LiFePO4: II. Particle size reduction and electrochemical evaluation. J Electrochem Soc 157(4):A463–A468
29. Daheron B, Macneil D (2011) Study of LiFePO4 synthesized using a molten method with varying stoichiometries. J Solid State Electrochem 15(6):1217–1225
30. Talebi-Esfandarani M, Rousselot S, Gauthier M, Sauriol P, Liang G, Dollé M (2015) LiFePO4 synthesized via melt process using low cost iron precursors. J Solid State Electrochem 20(7):1821–1829
31. Nishijima, M, Ootani, T, Kamimura, Y, Sueki, T, Esaki, S, Murai, S, Fujita, K, Tanaka, K, Ohira, K, Koyama, Y, and Tanaka, I (2014) Accelerated discovery of cathode materials with prolonged cycle life for lithium-ion battery. Nat Commun 5
32. Axmann P, Stinner C, Wohlfahrt-Mehrens M, Mauger A, Gendron F, Julien CM (2009) Nonstoichiometric LiFePO4: defects and related properties. Chem Mater 21(8):1636–1644
33. Brand, R 2008 WinNormos Software, Universität Duisburg-Essen, G. Duisbourg, Editor
34. Osterheld RK (1968) Liquidus diagram for the system lithium orthophosphate-lithium metaphosphate. J Inorg Nucl Chem 30(12): 3173–3175
35. Badi S-P, Wagemaker M, Ellis BL, Singh DP, Borghols WJH, Kan WH, Ryan DH, Mulder FM, Nazar LF (2011) Direct synthesis of nanocrystalline Li0.90FePO4: observation of phase segregation of anti-site defects on delithiation. J Mater Chem 21(27):10085–10093
36. Jensen KMØ, Christensen M, Gunnlaugsson HP, Lock N, Bøjesen ED, Proffen T, Iversen BB (2013) Defects in hydrothermally synthesized LiFePO4 and LiFe1-xMnxPO4 cathode materials. Chem Mater 25(11):2282–2290
37. Hamelet S, Gibot P, Casas-Cabanas M, Bonnin D, Grey CP, Cabana J, Leriche J-B, Rodriguez-Carvajal J, Courty M, Levasseur S, Carlach P, Van Thournout M, Tarascon J-M, Masquelier C (2009) The effects of moderate thermal treatments under air on LiFePO4-based nano powders. J Mater Chem 19(23):3979–3991
38. Andersson AS, Kalska B, Häggström L, Thomas JO (2000) Lithium extraction/insertion in LiFePO4: an X-ray diffraction and Mössbauer spectroscopy study. Solid State Ionics 130(1–2):41–52
39. Jensen KMØ, Gunnlaugsson HP, Christensen M, Iversen BB (2014) Mössbauer spectroscopy study of defects in hydrothermally synthesized $LiFePO_4$ cathode material. Hyperfine Interact 226:73–78
40. Maccario M, Croguennec L, Wattiaux A, Suard E, Le Cras F, Delmas C (2008) C-containing LiFePO4 materials—part I:

mechano-chemical synthesis and structural characterization. Solid State Ionics 179:2020–2026
41. Meethong N, Kao Y-H, Speakman SA, Chiang Y-M (2009) Aliovalent substitutions in olivine lithium iron phosphate and impact on structure and properties. Adv Funct Mater 19(7):1060–1070
42. Wagemaker M, Singh DP, Borghols WJH, Lafont U, Haverkate L, Peterson VK, Mulder FM (2011) Dynamic solubility limits in nanosized olivine LiFePO4. J Am Chem Soc 133(26):10222–10228
43. Lux SF, Lucas IT, Pollak E, Passerini S, Winter M, Kostecki R (2012) The mechanism of HF formation in LiPF6 based organic carbonate electrolytes. Electrochem Commun 14(1):47–50
44. Kang B, Ceder G (2009) Battery materials for ultrafast charging and discharging. Nature 458(7235):190–193
45. Kim JC, Li X, Kang B, Ceder G (2015) High-rate performance of a mixed olivine cathode with off-stoichiometric composition. Chem Commun 51(68):13279–13282